

Power Suppression and Lensing Anomaly – A phenomenological investigation

Roshna K^{*} and V. Sreenath[†]

Department of Physics, National Institute of Technology Karnataka, Surathkal, Mangaluru 575025, India.

Primordial power spectra with low power at long wavelengths can alleviate lensing anomaly. However the extent to which data favours such a primordial spectra is not clear. In this work, we investigate power suppression and related mitigation of lensing anomaly with the help of phenomenological models which are valid over scales of interest. We consider simple extensions to nearly scale invariant power spectra such as those which includes running and running of running of spectral index. We perform Bayesian analysis of these models, which are agnostic about power suppression, with various data sets and show that data tend to choose parameters which leads to power suppression at low multipoles. We then analyse the significance of these findings using information criteria. Further, we investigate the ability of near-ultimate future CMB missions such as ECHO to put tighter constraints on these models. We conclude that we can make stronger conclusions about the presence of power suppression in the future by studying such simple phenomenological models.

I. INTRODUCTION

Some of the most intriguing questions in cosmology concerns the *origin* of our Universe. For instance, we are yet to understand the exact mechanism that generated primordial perturbations that lead to the observed anisotropies and inhomogeneities in the Universe. Though inflationary scenario provides a very simple and elegant solution to this question, the question is far from settled. Questions concerning model of inflation, duration of inflation, tensor modes etc. are unresolved [1–5]. Further, we do not know much about our Universe close to the Planck regime.

A way to gain knowledge about the earliest epochs of our Universe is to study the imprints left by primordial perturbations generated then in cosmic microwave background (CMB). Since our Universe is expanding, physical wavelength of primordial perturbations which are generated early on in the universe expands more and leave their imprints at longer length scales. Hence, the largest angular scales or the lowest multipoles of the CMB contain valuable information about the early universe. Ever since the serendipitous discovery of CMB by Penzias and Wilson in 1964 [6], there have been several efforts to study CMB. The lowest multipoles of the CMB was first observed by COBE [7] satellite. These measurements were then refined considerably by both ground based and satellite missions. For a history of CMB measurements, see, for instance, [8]. The current state-of-the-art measurements of anisotropies, especially at low multipoles, in CMB has come from the Planck mission [9].

Bayesian studies of angular power spectra of CMB temperature and polarisation measured by Planck are in fairly good agreement with the predictions of standard model of cosmology especially so at high multipoles [1, 10]. However, there are certain signals at large angular scales in the CMB which depart mildly, at about 2 to $3-\sigma$, from the predictions of statistical isotropy and homogeneity by the standard model of cosmology. These mild departures from the predictions of standard model of cosmology are referred to as CMB anomalies [11, 12]. They include lack of power at large angular scales, dipolar modulation of low multipoles, alignment of low multipoles, preference for odd parity etc. These features are real, since they have been observed across different satellite missions and

^{*}Electronic address: roshnak.217ph005@nitk.edu.in

[†]Electronic address: sreenath@nitk.edu.in

hence are unlikely to be due to unmitigated instrumental noise. Further, even though individually they are mild departures from predictions of standard model, their combined occurrence makes them interesting. Even so, we can reason them away by considering our Universe to be a rather rare realization of the Universe predicted by standard model. However, we can be more *optimistic* and consider these anomalies to be signals of physics beyond standard model. Since physics of the early universe leave their imprints at low multipoles, there is a possibility that anomalies can be viewed as potential smoking guns of physics of early universe.

There have been several studies explaining ways a single CMB anomaly can arise from a primordial scenario. For instance there have been various works which investigate models which lead to suppression of power at large angular scales [13–17] (see also [18–21]), dipolar modulation [22], alignment of low multiples [23], quadrupolar modulation [24, 25] etc. If a single primordial mechanism can explain more than one anomalous feature in the CMB then the possibility that CMB anomalies are signals of primordial physics beyond the standard model becomes more credible. Recently, it was shown in the context of loop quantum cosmology that quantum effects could lead to a suppression of power at large angular scales which in turn could lead to lensing anomaly [26–28]. It was also proposed that non-Gaussian modulation could explain more than one anomaly including dipolar modulation, power suppression and lensing anomaly [29–31]. In this context see also, [32–37].

Lensing anomaly refers to an inconsistency in the estimation of value of lensing parameter from CMB. In particular, this refers to the fact that value of lensing parameter [38] seems to be different from the expected value of one. Lensing anomaly is different from other anomalies, in that effect of lensing is observed at large multipoles. In this work, we would like to investigate the existence of power suppression and explore the connection between power suppression and lensing anomaly from a phenomenological perspective. We shall assume simple extensions to nearly scale invariant primordial power spectrum such as the one which includes running and/or running of running of spectral index and investigate these anomalies. These models are agnostic about power suppression *i.e.* the parameters can take values which can lead to power suppression or an enhancement at low multipoles. We perform Bayesian parameter estimation and investigate whether data prefers values which lead to suppression of power at low multipoles. We then investigate the alleviation of lensing anomaly in these models. We discuss the significance of these findings using Akaike and Bayesian information criteria. We forecast the ability of near-perfect fourth generation CMB missions such as ECHO¹ (Exploring Cosmic History and Origins) to make tighter constraints on model parameters.

This paper is organised as follows. We begin with a brief review of essential aspects of standard model of cosmology, CMB data analysis and the anomalies of interest in section II. We describe the different analytical templates of primordial power spectrum, that we consider, in section III. In section IV, we perform a Bayesian parameter estimation of these models and investigate power suppression in them. We then explore the connection between power suppression and lensing anomaly in section V. In section VI, we discuss the extent to which these models are preferred by the data using information criteria. We then perform forecast for future CMB mission in section VII. We conclude the paper with a summary and a discussion of our results in section VIII.

II. STANDARD MODEL AND CMB ANOMALIES

Standard model of cosmology posits a spatially flat Friedmann-Lemaitre-Robertson-Walker geometry for our Universe with inhomogeneities seeded by Gaussian primordial perturbations [1, 39].

¹ <https://cmb-bharat.in/>

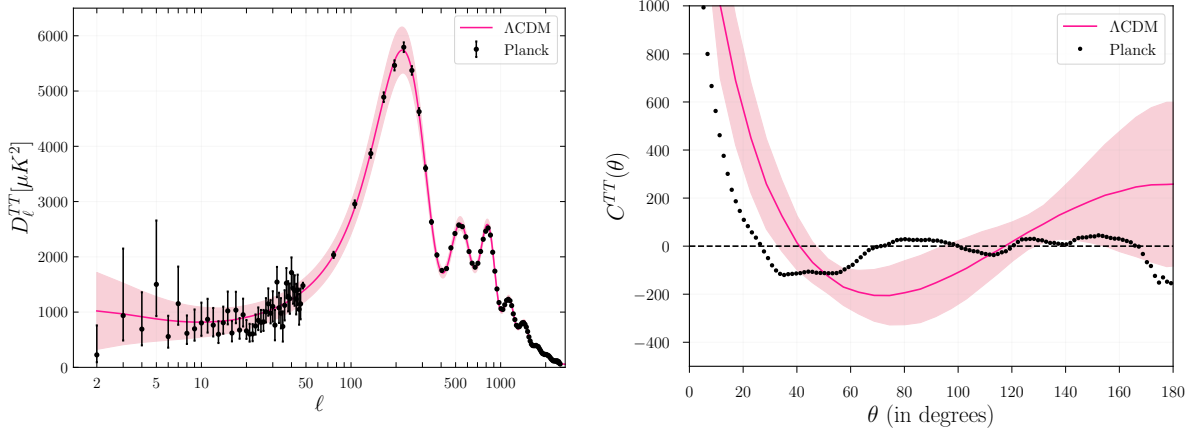


FIG. 1: The plots of D_ℓ^{TT} (left) and $C^{TT}(\theta)$ (right) corresponding to standard model. We have worked with marginalised mean values of parameters obtained using Bayesian parameter estimation with data of temperature, polarisation and lensing obtained by Planck.

According to this model, our Universe is mostly composed of cosmological constant (Λ) and cold dark matter (CDM). Hence, this model is also called as Λ CDM model [10]. With just six parameters Λ CDM model has been able to describe many aspects of our Universe quite well. The six parameters include energy density of baryons ($\Omega_b h^2$) and cold dark matter ($\Omega_c h^2$) – which describe the constitution of our Universe, hundred times the angle subtended by the sound horizon on the surface of last scattering ($100 \theta_{MC}$) – which describe the amount of expansion since last scattering, reionization depth (τ) – which informs us about the epoch of reionization and the amount of secondary anisotropies generated in the CMB and two parameters that describe the amplitude (A_s) and tilt (n_s) of the scalar primordial power spectrum, through the relation

$$\mathcal{P}_s(k) = A_s \left(\frac{k}{k_\star} \right)^{n_s - 1}. \quad (2.1)$$

We shall refer to this template for a nearly scale invariant power spectrum as the *Standard Ansatz* (SA). Such a power spectrum can be very easily generated in a large class of slow roll inflationary models.

Given a theoretical model, we can compute observables, gather data corresponding to these observables and compare both to arrive at information about model parameters. Because of the limitations inherent to the measurement, we cannot arrive at the exact values of the underlying model parameters. Bayes theorem provides a way to estimate the model parameters and to translate the errors in the measurement to our confidence in the estimated value (see, for instance, [40]). It can be stated as

$$P(\theta|D) = \frac{P(D|\theta) P(\theta)}{P(D)}, \quad (2.2)$$

where $P(\theta)$ is our prior knowledge about model parameters θ before carrying out the observation, $P(D|\theta)$ is the likelihood that data D will be obtained using the underlying model for the given values of parameters, $P(D)$ is a normalization constant or the evidence and $P(\theta|D)$ is the posterior probability distribution of model parameters. We can use stochastic methods such as Markov Chain Monte Carlo (MCMC) to sample the parameter space and arrive at the posterior probability distribution which captures our degree of belief in the value of model parameters.

Because of the mostly linear physics, anisotropies in the CMB provides one of the cleanest data to validate standard model. Hence, most of the current constraints on the standard model has been

arrived at using the data from CMB. In this paper we will first use state-of-the-art data measured by Planck for our analysis. Anisotropies present in the CMB are temperature fluctuations, electric or E-mode polarisation and magnetic or B-mode polarisation. Since temperature fluctuations and polarisation are random quantities, we can only compare their moments with the corresponding predictions from the model. Being the simplest, data of their variance or their power spectra as a function of multipole moments are used to constrain models. We use power spectra of temperature fluctuations (C_ℓ^{TT} or TT) and E-mode polarisation (C_ℓ^{EE} or EE) and their cross-correlation (C_ℓ^{TE} or TE). The B-mode polarisation from a primordial origin, though expected to be created by inflation, has not yet been detected. Lack of B-mode signal in CMB has helped us to rule out certain class of inflationary models. Another observable that has been derived from CMB is the power spectrum of lensing potential ($C_\ell^{\phi\phi}$). Using Boltzmann codes which allow us to compute these observables and using MCMC codes, we can compare a given model with data using Bayesian methods. In this article, we will work with **CosmoMC** [41] together with **CAMB** [42].

Figure 1 contains the plot (solid curve) of $D_\ell^{TT} = \ell(\ell+1) C_\ell^{TT}/2\pi$ generated by standard model with parameters set to their marginalised mean values obtained from a Bayesian comparison with Planck data. Dots with error bars represent data observed by Planck. These error bars arise due to limitations in the measurement. Cosmic variance is indicated by the shaded region. Unlike other measurement errors which can be minimised by improving the instrument, cosmic variance is an inherent limitation of cosmological measurements. It arises due to the fact that while taking averages we cannot take ensemble average neither can we do a spatial average. In the context of C_ℓ^{XY} , where X and Y are either temperature fluctuations or E-mode polarisation, this implies that we can only average over m values of harmonic coefficients. Cosmic variance of C_ℓ^{XY} is $\sqrt{2/(2\ell+1)}C_\ell^{XY}$. Hence, the uncertainty due to cosmic variance is more at low multipoles. Due to galactic foreground and other point sources, Planck has only observed a fraction of the sky. To account for this, we have scaled the cosmic variance by f_{sky}^{-1} , where fraction of sky observed by Planck $f_{sky} = 0.86$ ². As is clear from the figure 1, the standard model provides a fairly good fit to the Planck data. However, there are some features in the CMB that deviate from predictions of standard model. In the remaining part of this section, we will focus on some of these features.

We will mainly consider two anomalies. Firstly, the observed power of temperature fluctuations at low multipoles is lower than that predicted by the standard model. This lack of power is more evident if we plot CMB spectrum in terms of angular separation. The angular power spectrum of temperature fluctuations generated in the standard model is plotted in the right panel of figure 1. In terms of C_ℓ^{TT} it is given by

$$C^{TT}(\theta) = \frac{1}{4\pi} \sum_{\ell} (2\ell + 1) C_\ell^{TT} P_\ell(\cos \theta). \quad (2.3)$$

The shaded region represents the cosmic variance and the black dots represents the observations. From the plot, we can see that while the data for angles greater than 60° is quite close to zero, the solid curve that corresponds to the standard model is not. This lack of power at large angular scales can be quantified using [44]

$$S_{1/2} = \int_{-1}^{1/2} C(\theta)^2 d(\cos \theta). \quad (2.4)$$

The value of $S_{1/2}$ observed by Planck is 1209 [12] compared to 34810 obtained with the marginalised mean values for standard model.

² Value of f_{sky} varies with choice of foreground mask [43].

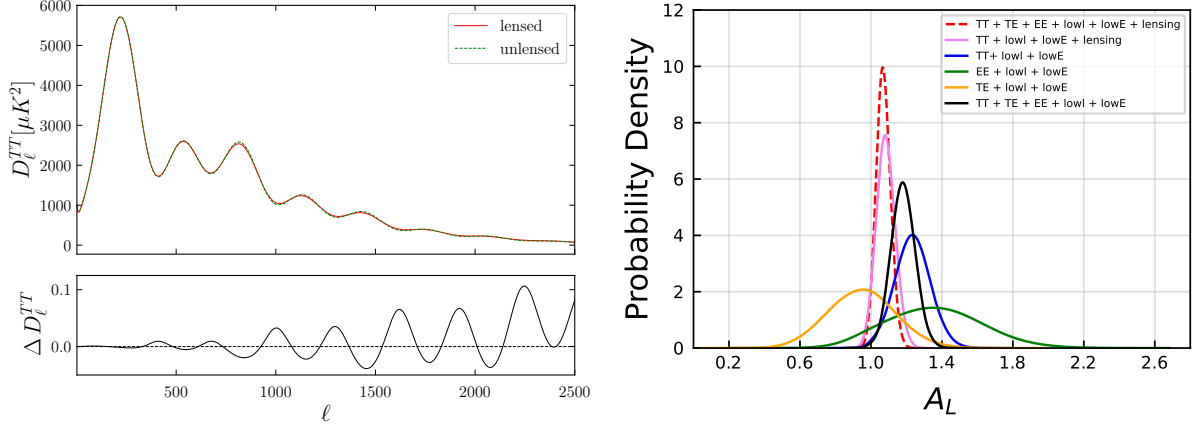


FIG. 2: Effect of lensing on D_ℓ^{TT} (left) and marginalised posterior probability density of A_L (right) is plotted. The effect of lensing is more prominent at high multipoles as clearly demonstrated in the lower subplot on the left panel. Here, ΔD_ℓ^{TT} refers to ratio of difference between lensed and unlensed D_ℓ^{TT} divided by lensed D_ℓ^{TT} . In obtaining the plots in the left panel, we have worked with same parameter values as in figure 1. The right panel was obtained by Bayesian estimation of A_L along with the usual six parameters with Planck data.

CMB as it travels to us get weakly lensed by intervening structure. The effect of this lensing is, see figure 2, a smoothening of acoustic peaks that is primarily felt at large multipoles or low angular scales. The effect of the lensing in the spectra of temperature anisotropies and polarisation should be consistent with the spectra of lensing potential. To check this consistency, WMAP [38] team had introduced a lensing parameter A_L that multiplies the power spectra of lensing potential. If we treat A_L as a free parameter and do a Bayesian analysis by comparing the resultant seven parameter model, *i.e.* A_L and the usual six parameters, with Planck temperature and polarisation data, the constraints on A_L should be consistent with one. Such a result would imply that we have accounted for the effects of lensing correctly. The results of such an analysis, provided in the right panel of figure 2, indicate otherwise. We find that the value of A_L is consistent with one within $2 - \sigma$, only if we include data of lensing potential [10]. For instance, if we work with TT data alone, then the marginalised mean value of A_L turns out to be $A_L = 1.24 \pm 0.09$ which is much more than $2 - \sigma$ away from the value of one.

We now proceed to investigate power suppression at low multipoles and its connection with lensing anomaly using certain phenomenological models. We begin by presenting these models in the next section.

III. EXTENSIONS TO STANDARD MODEL

To investigate the connection between primordial physics and CMB anomalies, in addition to the nearly scale invariant form of power spectrum, we will also consider certain extended templates of primordial power spectrum. The remaining four parameters in the Λ CDM model will remain unchanged. The models that we consider in this work are described below.

A. Nearly scale invariant model with running of spectral index

In this model we consider running of the spectral index, *i.e.*

$$\mathcal{P}_{\mathcal{R}}(k) = A_s \left(\frac{k}{k_{\star}} \right)^{n_s - 1 + \frac{1}{2} \alpha \ln(k/k_{\star})}. \quad (3.1)$$

Including running of spectral index (α), this model thus contains seven parameters. We will refer to this model as $SA + \alpha$.

B. Nearly scale invariant model with running and running of running of spectral index

In this model, in addition to running of the spectral index, we consider running of running *i.e.*

$$\mathcal{P}_{\mathcal{R}}(k) = A_s \left(\frac{k}{k_{\star}} \right)^{n_s - 1 + \frac{1}{2} \alpha \ln(k/k_{\star}) + \frac{1}{6} \beta \ln(k/k_{\star})^2}. \quad (3.2)$$

Including running of spectral index (α) and running of running of spectral index (β), in addition to the standard model, this model thus contains eight parameters. We will refer to this model as $SA + \alpha + \beta$.

C. Nearly scale invariant model with running of running of spectral index

In this model, we consider only running of running to the standard nearly scale invariant power spectrum. *i.e.*

$$\mathcal{P}_{\mathcal{R}}(k) = A_s \left(\frac{k}{k_{\star}} \right)^{n_s - 1 + \frac{1}{6} \beta \ln(k/k_{\star})^2}. \quad (3.3)$$

Including running of running of spectral index (β), in addition to the standard model, this model thus contains seven parameters. We will refer to this model as $SA + \beta$.

It should be highlighted that, in this analysis, we do not assume that these phenomenological models describe the full behaviour of primordial power spectrum valid over the entire wavelength range. For instance, the values of α and β in the $SA + \alpha + \beta$ model that favour power suppression at long wavelengths lead to enhancement in power at short wavelengths. However, we are only interested in the ability of this model to describe power suppression at long wavelengths. With this in mind, we will restrict ourselves to CMB data of multipoles less than $\ell \lesssim 2500$.

IV. POWER SUPPRESSION IN EXTENSIONS TO STANDARD MODEL

We now employ Bayesian parameter estimation to find out the value of parameters of SA , $SA + \alpha$, $SA + \alpha + \beta$ and $SA + \beta$ models. We will show that the value of model parameters preferred by the data leads to a suppression of power at large angular scales. As mentioned in section II, we have used **CosmoMC** together with **CAMB** for this analysis. In this work, we have assumed a flat prior for all parameters as described in table I. We have compared these models with a variety of data sets. The most accurate data that we have is that of temperature anisotropies measured by Planck [10]. It is in fact one of the best measured observable of our universe. The error bars for this data are better than that due to cosmic variance. Planck's measurement of temperature

Parameter	Prior
$\Omega_b h^2$	[0.005, 0.1]
$\Omega_c h^2$	[0.001, 0.99]
$100 \theta_{\text{MC}}$	[0.5, 10]
τ	[0.01, 0.8]
$\ln(10^{10} A_s)$	[1.61, 3.91]
n_s	[0.8, 1.2]
α	[-1, 1]
β	[-1, 1]
A_L	[0, 2.7]

TABLE I: Table lists the range of values of different parameters, appearing in various models, over which a uniform prior knowledge is assumed.

	SA	$SA + \alpha$	$SA + \beta$	$SA + \alpha + \beta$
$\Omega_b h^2$	0.0221 ± 0.00022	0.0222 ± 0.00023	0.0221 ± 0.00022	0.022 ± 0.00027
$\Omega_c h^2$	0.1206 ± 0.00209	0.1207 ± 0.00212	0.1216 ± 0.0022	0.1221 ± 0.0022
$100 \theta_{\text{MC}}$	1.0408 ± 0.00047	1.0408 ± 0.00047	1.0407 ± 0.00047	1.0406 ± 0.00048
τ	0.0517 ± 0.0080	0.0531 ± 0.0086	0.0554 ± 0.0087	0.0545 ± 0.0088
$\ln(10^{10} A_s)$	3.04 ± 0.016	3.04 ± 0.018	3.05 ± 0.018	3.05 ± 0.019
n_s	0.9627 ± 0.0057	0.9620 ± 0.0059	0.9573 ± 0.0067	0.9551 ± 0.0069
α	0	-0.0040 ± 0.0076	0	0.0136 ± 0.0125
β	0	0	0.0133 ± 0.0089	0.0256 ± 0.0142
χ^2	1192.1 ± 5.5	1192.9 ± 5.7	1191 ± 5.6	1190.5 ± 5.8

TABLE II: Marginalised mean and standard deviation of different model parameters obtained by Bayesian parameter estimation. In this analysis, we have worked with TT + low ℓ + low E data. Last row of this table contain the marginalised mean and standard deviation of values of χ^2 obtained from the posterior distribution.

fluctuations is available over the multipoles $\ell = [2, 2508]$. While working with temperature data, we have also included low ℓ EE data (**small**). This is done to obtain better constraints on reionization depth [43]. Following Planck’s notation, we will refer to this data set as TT + lowl + lowE. The results of Bayesian parameter estimation are provided in table II.

We also consider the effect of including polarisation data from high multipoles. In particular, along with temperature and low multipole EE spectrum, we consider TE and EE spectra from multipoles 30 – 1996. We shall refer to this data set as TTTEEE + lowl + lowE. Marginalised mean values and standard deviation of cosmological parameters for various models obtained from their posterior probability distributions are tabulated in table III.

Finally, we also extend the analysis of our models to include non-CMB data. In particular, we include measurements of the Baryon Acoustic Oscillations (BAO) data obtained from 6DF [45], MGS [46] and SDSS surveys [47]. We also include first year release of data of galaxy clustering and weak lensing from Dark Energy Survey (DES) [48–50]. We shall refer to this data set as Planck + BAO + DES. Results of Bayesian parameter estimation upon working with TT + lowl + lowE + BAO + DES and Planck + BAO + DES data sets are given in tables IV and V respectively.

On the left panel of figure 3, D_ℓ^{TT} is plotted as a function of multipoles. In obtaining this plot, we have worked with the marginalised mean values of cosmological parameters obtained by comparing models with TT + lowl + lowE data. Figure illustrates that power at lower multipoles for the extended models is lower in amplitude compared to that generated in SA . This is much

	SA	$SA + \alpha$	$SA + \beta$	$SA + \alpha + \beta$
$\Omega_b h^2$	0.0224 ± 0.00015	0.0224 ± 0.00016	0.0224 ± 0.00015	0.0223 ± 0.00016
$\Omega_c h^2$	0.1202 ± 0.00136	0.1204 ± 0.00140	0.1206 ± 0.00142	0.1207 ± 0.00142
$100 \theta_{MC}$	1.0409 ± 0.00031	1.0409 ± 0.00032	1.0409 ± 0.00031	1.0409 ± 0.00032
τ	0.0544 ± 0.0078	0.0559 ± 0.0081	0.0573 ± 0.0085	0.0575 ± 0.0087
$\ln(10^{10} A_s)$	3.04 ± 0.0159	3.05 ± 0.0170	3.05 ± 0.0175	3.05 ± 0.0180
n_s	0.9649 ± 0.0043	0.9634 ± 0.0047	0.9614 ± 0.0051	0.9612 ± 0.0052
α	0	-0.0062 ± 0.0068	0	0.0011 ± 0.0102
β	0	0	0.0102 ± 0.0084	0.0117 ± 0.0127
χ^2	2780.2 ± 5.8	2780.8 ± 6.0	2779.8 ± 5.9	2780.9 ± 6.1

TABLE III: Marginalised mean value and standard deviation of cosmological parameters obtained by Bayesian analysis of models with TTTEEE + lowl + lowE data. Mean and standard deviation of χ^2 obtained from the posterior distribution is listed in the last row.

	SA	$SA + \alpha$	$SA + \beta$	$SA + \alpha + \beta$
$\Omega_b h^2$	0.0223 ± 0.00019	0.0223 ± 0.00021	0.0223 ± 0.00019	0.0222 ± 0.00023
$\Omega_c h^2$	0.1174 ± 0.00101	0.1174 ± 0.00101	0.1175 ± 0.00101	0.1175 ± 0.00102
$100 \theta_{MC}$	1.0411 ± 0.00041	1.0411 ± 0.00041	1.0411 ± 0.000419	1.0411 ± 0.000412
τ	0.0527 ± 0.0079	0.0530 ± 0.0082	0.0555 ± 0.0086	0.0550 ± 0.0087
$\ln(10^{10} A_s)$	3.03 ± 0.0161	3.03 ± 0.0173	3.04 ± 0.0175	3.04 ± 0.0181
n_s	0.9694 ± 0.0040	0.9693 ± 0.0042	0.9669 ± 0.0046	0.9656 ± 0.0047
α	0	-0.00064 ± 0.0074	0	0.0147 ± 0.0121
β	0	0	0.0091 ± 0.0084	0.0220 ± 0.0137
χ^2	1717.4 ± 7.4	1718.3 ± 7.5	1717.2 ± 7.5	1716.4 ± 7.8

TABLE IV: Marginalised mean and standard deviation of cosmological parameters obtained by a Bayesian analysis of models with TT + lowl + lowE + BAO + DES data. Mean and standard deviation of χ^2 obtained from the posterior distribution is listed in the last row.

more evident in the plot of corresponding angular power spectra, Eqn. (2.3), plotted on the right side of the same figure. Figure illustrates that at angular scales larger than 60° , power is lesser for the extended models. The lack of power at large angular scales is quantified by the $S_{1/2}$, see Eqn. (2.4), values listed in table VI. Unlike figure 3, table not only lists the values of $S_{1/2}$ corresponding to the marginalised mean values derived from TT + lowl + lowE data given in table II, but also shows the values corresponding to analysis performed with other data sets listed in tables III, IV and V. Note that lower value of $S_{1/2}$ implies lower power at large angular scales. Table indicates that for all extensions to standard model considered in this paper, data chooses parameters that lead to a lowering of $S_{1/2}$ or equivalently leads to power suppression at large angular scales. This is the first result of this paper. We note that power suppression is largest for $SA + \alpha + \beta$ model. The $SA + \beta$ model also lead to a comparable, but slightly higher, value of $S_{1/2}$. The value of $S_{1/2}$ for $SA + \alpha$ is only slightly smaller than that generated in SA . It is interesting to note that when polarisation data is considered the value of $S_{1/2}$ increases in all models except $SA + \alpha$. On the other hand, when BAO and DES data are considered in addition to TT + lowl + lowE data, value of $S_{1/2}$ increases for all models except for the case of SA . A similar behaviour is observed when BAO and DES are added to Planck data.

	SA	$SA + \alpha$	$SA + \beta$	$SA + \alpha + \beta$
$\Omega_b h^2$	0.0225 ± 0.00013	0.0225 ± 0.00014	0.0225 ± 0.00013	0.0225 ± 0.00014
$\Omega_c h^2$	0.1180 ± 0.00087	0.1180 ± 0.00087	0.1181 ± 0.00090	0.1181 ± 0.00088
$100 \theta_{MC}$	1.0411 ± 0.00029	1.0411 ± 0.00029	1.0411 ± 0.00029	1.0411 ± 0.00029
τ	0.0541 ± 0.0078	0.0548 ± 0.0079	0.0562 ± 0.0083	0.0565 ± 0.0083
$\ln(10^{10} A_s)$	3.04 ± 0.016	3.04 ± 0.016	3.04 ± 0.017	3.04 ± 0.017
n_s	0.9693 ± 0.0037	0.9688 ± 0.0039	0.9674 ± 0.0043	0.9671 ± 0.0043
α	0	-0.0025 ± 0.0067	0	0.0045 ± 0.0102
β	0	0	0.0069 ± 0.0083	0.0113 ± 0.0125
χ^2	3306.1 ± 7.7	3306.9 ± 7.9	3306.3 ± 7.9	3307.0 ± 8.1

TABLE V: Marginalised mean and standard deviation of cosmological parameters obtained by a Bayesian analysis of models with Planck + BAO + DES data. Mean and standard deviation of χ^2 obtained from the posterior distribution is listed in the last row.

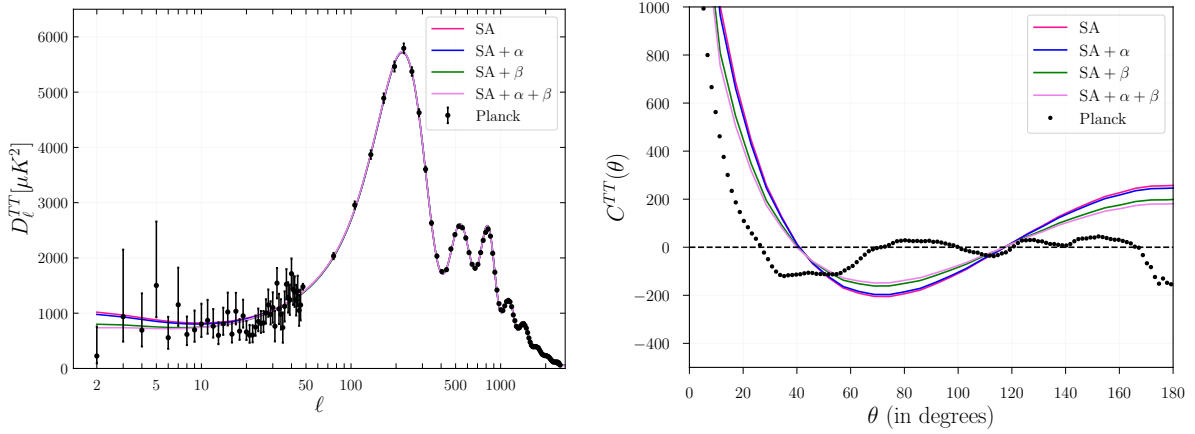


FIG. 3: Plots of D_ℓ^{TT} as a function of multipoles (left) and of $C^{TT}(\theta)$ (right) corresponding to different models are given. We have worked with marginalised mean values of parameters given in table II which were obtained by comparing models with TT + lowl + lowE data. Figure illustrates that data prefers parameter values that lead to suppression in power at low multipoles or at large angles.

	SA	$SA + \alpha$	$SA + \beta$	$SA + \alpha + \beta$
TT + lowl + lowE	34646	31878	21064	17699
TTTEEE + lowl + lowE	34834	30640	23721	22990
TT + lowl + lowE + BAO + DES	34336	33907	24611	20795
Planck + BAO + DES	34513	32743	26600	24909

TABLE VI: Values of $S_{1/2}$ corresponding to different models is tabulated in different columns of this table. $S_{1/2}$ was obtained by evaluating Eqn. (2.4). Different rows corresponds to marginalised mean values of model parameters obtained with different data sets as given in tables II, III, IV and V.

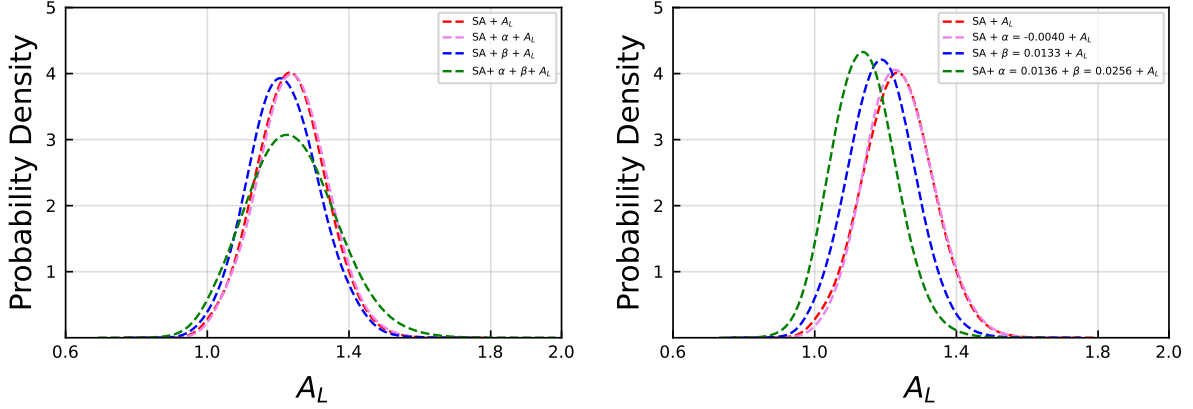


FIG. 4: Plot of marginalised probability distribution of A_L for all four models. This plot was derived from the posterior probability distribution of model parameters obtained by comparing models with TT + lowl + lowE data. Plot on the left was obtained by varying all model parameters, whereas in obtaining the plot on the right, we have fixed the values of α and β to their respective mean values in table II.

V. CONNECTION BETWEEN POWER SUPPRESSION AND LENSING ANOMALY

We now investigate the connection between suppression of power at large angular scales and the lensing anomaly. In earlier works, it was shown, in the context of loop quantum cosmology, that a primordial power spectra with a lack of power at long wavelengths could alleviate lensing anomaly [26–28]. In this section, we investigate the extent to which lensing anomaly gets resolved in these extensions to standard model. We perform two types of analysis.

In first, we perform Bayesian parameter estimation for the three extensions to standard model after including the lensing parameter (A_L) as a free parameter. This extends the number of free parameters in each model by one. We have worked with TT + lowl + lowE data. Marginalised posterior probability distribution of the lensing parameter A_L , obtained using this approach is plotted in the left side of figure 4. We can see from the figure that the probability distribution becomes broader for $SA + \beta$ and $SA + \alpha + \beta$ model. Thus, the value of $A_L = 1$ become more probable. This point is more clear if we look at the table VII which tabulates the mean and standard deviation of A_L for different models. Note that, in $SA + \alpha + \beta$ model, though mean value $A_L = 1$ remains the same as that in SA , its standard deviation is larger, making the value of $A_L = 1$ within $2 - \sigma$. In the case of $SA + \beta$ model, the mean value of A_L is slightly lower and the standard deviation is slightly larger making the value of $A_L = 1$ more probable. The constraints on A_L in both SA and $SA + \alpha$ models are largely similar.

In the second approach, we fix values of α and β to those given in table II and then vary the remaining parameters of the model along with lensing parameter. The marginalised mean and standard deviation of the lensing parameter is given in the second row of table VII. The mean value of lensing parameter obtained in the $SA + \alpha + \beta$ model is considerably smaller than that obtained for SA . This brings the value $A_L = 1$ well within $2 - \sigma$ range. We also find that the value of A_L is lower for $SA + \beta$ model making the value of $A_L = 1$ more probable. As in the first method, we find that constraints on A_L in both SA and $SA + \alpha$ models are largely similar. To summarize, both methods show that the extended models which lead to power suppression also makes the value of $A_L = 1$ more probable and thus making it less anomalous. This is the second result of this paper.

It is interesting to ask what happens if we include additional data in our analysis. To answer this, we shall focus on models $SA + \beta$ and $SA + \alpha + \beta$ and work with data sets TTTEE + lowl

	SA	$SA + \alpha$	$SA + \beta$	$SA + \alpha + \beta$
Method I	1.240 ± 0.094	1.246 ± 0.096	1.221 ± 0.100	1.242 ± 0.126
Method II	-	1.242 ± 0.096	1.194 ± 0.091	1.142 ± 0.091

TABLE VII: Marginalised mean and standard deviation of A_L corresponding to different models are tabulated. We have worked with TT + lowl + lowE data. In Method I, all model parameters are varied along with lensing parameter, whereas in Method II, we have fixed the value of α and β to those mentioned in table II. Both methods show that lensing anomaly is alleviated for models $SA + \beta$ and $SA + \alpha + \beta$.

+ lowE, TT + lowl + lowE + BAO + DES and Planck + BAO + DES. The results of this analysis are given in table VIII.

When we consider additional data sets, we observe that the mean values of A_L as well as its error bars are smaller. When we include CMB polarisation data, we note that the mean values of A_L obtained for $SA + \beta$ and $SA + \alpha + \beta$ are lower than that obtained for SA . This is true regardless of whether we fix the values of α and β to their marginalised mean values or not. However alleviation of lensing anomaly is more in the case where α and β are fixed as per table III. When we consider the data set TT + lowl + lowE + BAO + DES, we observe that BAO and DES data sets do not affect the mean value of A_L . This is evident from a comparison of mean values of A_L given in tables VII and VIII for the case of SA . However inclusion of BAO and DES reduces the error bars causing a worsening of lensing anomaly. The expected value of one for the lensing parameter is more than $3 - \sigma$ away for SA . Analysis using first method shows that $A_L = 1$ comes within $3 - \sigma$ for $SA + \alpha + \beta$ model. This is also observed in analysis using second method. Though the mean value of A_L observed for $SA + \beta$ model is slightly lower than SA , the alleviation of lensing anomaly is lesser than that observed in $SA + \alpha + \beta$. We also consider a combination of data sets used in the previous two analysis, *i.e.* Planck + BAO + DES. Recall that Planck refers to high- ℓ TTTEEE along with lowl + lowE. Though there is a lowering of mean value of A_L , it is minimal. Consistent with rest of the analysis, lowering of A_L is observed most in the $SA + \alpha + \beta$ model when α and β are fixed to their marginalised mean values. This analysis shows that the alleviation of lensing anomaly weakens when additional data is included. The alleviation of lensing anomaly is best observed in analysis of TT + lowl + lowE data. It is interesting to compare this with the observations of table VI which shows that $S_{1/2}$ value and hence suppression is most evident in analysis with TT + lowl + lowE data. Thus, power suppression is indeed connected to alleviation of lensing anomaly. Larger the suppression, better is the alleviation of lensing anomaly. At the close of this section it should be remarked that E mode polarisation and data from large scale structure have not been measured as well as the temperature anisotropy. So, a higher value of $S_{1/2}$ and hence a lesser amount of alleviation of lensing anomaly favoured by these additional data do not necessarily indicate absence of these effects. A more refined measurement, particularly of E mode polarisation may be needed to make a more concrete statement about power suppression at large angular scales. We will make forecasts for such a measurement in section VII.

VI. SIGNIFICANCE OF RESULTS

A relevant question in this analysis concerns the significance of lack of power on large scales to warrant the addition of extra parameters such as α and β . To study the significance with which the extensions to the standard model are favoured, we consider two criteria namely the Akaike Information Criterion (AIC) [51] and Bayesian Information Criterion (BIC) [52]. AIC and BIC are

		SA	$SA + \beta$	$SA + \alpha + \beta$
TTTEEE + lowl + lowE	Method I	1.183 ± 0.068	1.174 ± 0.068	1.180 ± 0.070
	Method II	-	1.164 ± 0.066	1.161 ± 0.066
TT + lowl + lowE + BAO + DES	Method I	1.240 ± 0.075	1.233 ± 0.076	1.226 ± 0.080
	Method II	-	1.231 ± 0.075	1.203 ± 0.074
Planck + BAO + DES	Method I	1.204 ± 0.060	1.203 ± 0.060	1.199 ± 0.061
	Method II	-	1.200 ± 0.060	1.195 ± 0.060

TABLE VIII: Marginalised mean and standard deviation of A_L corresponding to different models when compared with additional data sets are tabulated. As in previous table results obtained using two different methods are given.

defined as follows,

$$AIC = 2n - 2 \ln \mathcal{L}, \quad (6.1)$$

$$BIC = n \ln N - 2 \ln \mathcal{L}, \quad (6.2)$$

where n is the total number of free parameters in a given model, N is the number of data points and \mathcal{L} is the maximum value of likelihood function for a given choice of model and data. The above definitions indicate that BIC penalise addition of extra parameters much more than AIC. We obtain the maximum likelihood required for computing AIC and BIC using Powell's bounded minimization routine (`action = 2`) of `CosmoMC`. For these analyses, we assume a flat prior as described in table I. We work with SA as the reference model. Since, power suppression and hence alleviation of lensing anomaly is more observed in $SA + \beta$ and $SA + \alpha + \beta$ models, we restrict our attention to them. As in the previous sections, we work with various combination of data sets. We note that TT + lowl + lowE contains 2535, TTTEEE + lowl + lowE contains 6469, TT + lowl + lowE + BAO + DES contains 3443 and Planck + BAO + DES contains 7377 data points respectively. The number of model parameters includes nuisance parameters. This is different for each data set. They are 21, 27, 41 and 47 for SA when working with TT + lowl + lowE, TTTEEE + lowl + lowE, TT + lowl + lowE + BAO + DES and Planck + BAO + DES respectively. Models $SA + \beta$ and $SA + \alpha + \beta$ has one and two extra parameters, respectively. The results of this analysis are given in table IX.

According to these information criteria [53, 54] if the difference in AIC (BIC) of a model being tested with respect to the reference model, ΔAIC (ΔBIC), is between $[0, 2]$ then it indicates a weak preference for the reference model. If ΔAIC (ΔBIC) is between $(2, 6]$ then it indicates a moderate preference for the reference model. A ΔAIC (ΔBIC) greater than 6, indicates a strong preference for the reference model. The table IX lists χ^2 corresponding to the best fit value for different models obtained upon comparison with various data sets and values of ΔAIC and ΔBIC derived from it. Our calculations of ΔAIC indicate a weak preference for SA compared to its extensions when polarisation data is not included. When polarisation is included, SA becomes moderately favoured compared to $SA + \alpha + \beta$ model. Compared to the $SA + \beta$ model, the preference for SA remains weak even when high- ℓ polarisation data is included. The addition of BAO or DES does not seem to considerably affect our estimates of AIC. This indicates that BAO or DES data do not constrain α or β much.

Data	Model	χ^2	Δ AIC	Δ BIC
TT + lowl + lowE	SA	1180.1202	0	0
	$SA + \beta$	1178.4433	0.3230	6.161
	$SA + \alpha + \beta$	1176.7702	0.649	12.325
TTTEEE + lowl + lowE	SA	2766.0492	0	0
	$SA + \beta$	2764.8400	0.7908	7.565
	$SA + \alpha + \beta$	2764.4662	2.416	15.966
TT + lowl + lowE + BAO + DES	SA	1699.2963	0	0
	$SA + \beta$	1697.6208	0.324	6.468
	$SA + \alpha + \beta$	1695.5091	0.212	12.501
Planck + BAO + DES	SA	3285.5571	0	0
	$SA + \beta$	3284.3935	0.836	7.742
	$SA + \alpha + \beta$	3284.3009	2.743	16.555

TABLE IX: Table of Δ AIC and Δ BIC of SA , $SA + \beta$ and $SA + \alpha + \beta$ computed using formulae 6.1, 6.2. We have set SA as the reference model. χ^2 was estimated using Powell's bounded minimization scheme.

According to BIC criterion, data strongly favours SA model when working with TT + lowl + lowE data. The addition of high- ℓ polarisation data improves the preference. However, as in the case of AIC, addition of BAO or DES data sets does not improve the preference much. The strong preference for SA when using BIC can be attributed to its dependence on the number of data points. BIC penalises addition of parameters through the term $n \ln N$ compared to $2n$ for AIC. This implies that larger the number of data points higher will be the penalty for adding extra parameters. This would be understandable if we were introducing extra parameters to describe a feature which is present in all the data points. However, the feature of our interest is a lack of power that is limited to low multipoles. Hence, while considering BIC to select models which differ by a local feature, it is more reasonable to work with data points which are centered around the feature³. In table X we have computed Δ AIC and Δ BIC with data limited to lowl. Table indicates weak preference for SA when compared with $SA + \beta$ model and a moderate preference for SA when compared with $SA + \alpha + \beta$ model. Lower values of Δ AIC (Δ BIC) of $SA + \beta$ compared to $SA + \alpha + \beta$ can be attributed to it having one less parameter. Significance of models summarized in tables IX and X is the third result of this paper.

³ To find out whether a cobra has eaten a frog, we just need to look at its belly.

Data	Model	χ^2_{lowl}	Δ AIC	Δ BIC
	SA	23.317	0	0
TT + lowl + lowE	$SA + \beta$	21.467	0.150	1.481
	$SA + \alpha + \beta$	22.026	2.707	5.372

TABLE X: The Δ AIC and Δ BIC is computed for lowl data. The table indicates that AIC weakly prefers SA when compared with $SA + \beta$ and moderately prefers SA compared to $SA + \alpha + \beta$. Preference for SA is weak when BIC is used to compare with $SA + \beta$ and moderate when compared with $SA + \alpha + \beta$.

VII. FORECAST FOR FUTURE CMB MISSIONS

Bayesian parameter estimation with TT + lowl + lowE constraints $\alpha = 0.0136 \pm 0.0125$ and $\beta = 0.0256 \pm 0.0142$ (see table II). Though mean value indicates a model which leads to a lack of power at low multipoles, the error bars are quite large with $\alpha = \beta = 0$ lying within $2-\sigma$ error bar. Planck satellite has measured temperature anisotropies to great accuracy and it is now only limited by cosmic variance. However this is not the case for polarisation. In this section, we investigate whether a future CMB mission which measures polarisation to a better extent can arrive at tighter constraints on α and β . For our analysis we shall consider ECHO, a fourth-generation satellite mission proposal for a near-ultimate measurements of the polarisation and discovery of global CMB spectral distortions submitted to Indian Space Research Organisation⁴. ECHO is similar in spirit to other proposed fourth-generation satellite missions such as CORe [55], PRISM [56] and PICO [57].

In order to forecast the extent to which a mission can constrain parameters of a model, we need an estimate of instrument noise. Following [58, 59], we shall assume a uniform instrumental noise and a Gaussian beam. If we assume that the detector observes f_{sky} fraction of the sky, then power spectrum of white noise of a detector that measures temperature anisotropy for a given frequency channel ν is given by

$$N_{T,\ell}^\nu = \frac{4\pi f_{sky} \sigma_{pix}^2}{N B_\ell(\theta_b)^2} = \frac{\Omega_{pix} f_{sky} \sigma_{pix}^2}{B_\ell(\theta_b)^2} \quad (7.1)$$

in units of $\mu K^2.sr$. In the above expression, $B_\ell(\theta_b) = \exp(-\ell(\ell+1)\theta_b^2/2)$ is the beam function of a Gaussian beam with standard deviation θ_b . If the full-width at half maximum of the beam is θ_{FWHM} , then $\theta_b = \theta_{FWHM}/\sqrt{8\ln 2}$. We consider N pixels and the area of a pixel is taken to be that of a square of side θ_{FWHM} , i.e. $\Omega_{pix} = \theta_{FWHM} \times \theta_{FWHM}$. σ_{pix} refers to the root mean square noise per pixel. The total noise from all frequency channels is [60],

$$N_{T,\ell} = \frac{1}{\sum_\nu 1/N_{T,\ell}^\nu}. \quad (7.2)$$

The power spectrum of noise in the polarisation channel is related to that in the temperature channel by $N_{E,\ell} \propto N_{T,\ell}$, where in the proportionality constant is two for near-ultimate missions such as ECHO and four for Planck.

⁴ <https://www.isro.gov.in>

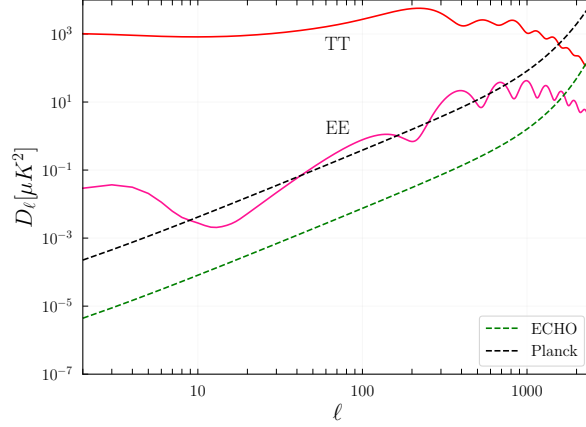


FIG. 5: Scale invariant noise power spectra for ECHO and Planck satellites. D_ℓ^{TT} and D_ℓ^{EE} are given for reference. Note that measurement of E-mode polarisation by ECHO satellite will be near perfect and only be limited by cosmic variance.

The scale invariant spectra of noise in the polarisation channel, $\ell(\ell+1)N_{E,\ell}/2/\pi$ for ECHO and Planck missions, for a sky fraction $f_{sky} = 0.7$, are given in figure 5. For this, we have used the values of ΔT and θ_{FWHM} provided in the proposal by CMB-Bhārat consortium (also given in table 1 of [61]). ECHO has a total of 20 frequency channels for measuring polarisation. We consider five frequency channels in the range 100-200 GHz which we consider as relevant for extracting cosmological information. For obtaining noise spectra of Planck, we have worked with values of $\Delta T/T$, where $T = 2.726\text{K}$ is the CMB temperature, and θ_{FWHM} provided in the Planck blue book (table 1.1 of [62]). Out of the nine frequency channels, we focus on channels with frequency 100 GHz, 143 GHz and 217 GHz that are relevant for cosmology. The ΔT is related to σ_{pix} through $\sigma_{pix} = \Delta T \times \theta_{FWHM}$. We have also plotted the cosmic variance limited signal D_ℓ^{TT} and D_ℓ^{EE} for reference. In obtaining these curves, we have assumed SA model with parameter values set to marginalised mean values obtained up on comparison with $TT + \text{lowl} + \text{lowE}$ as the fiducial model (see table II).

To forecast achievable constraints on α and β with ECHO mission, along with the above noise model, we work with two fiducial cosmologies. Firstly, we consider angular power spectra generated with SA model with parameter values set to their marginalised mean values obtained up on comparison with $TT + \text{lowl} + \text{lowE}$, see table II. We refer to this data as Fiducial Cosmology I (FC-1). This model implies no suppression of power at low multipoles. Secondly, we consider angular power spectra generated by $SA + \alpha + \beta$ model with parameter values set to marginalised mean values obtained up on comparison with $TT + \text{lowl} + \text{lowE}$, see table II. We refer to it as Fiducial Cosmology II (FC-2). Forecasts for α and β are obtained using Bayesian parameter estimation with data described by the fiducial cosmology and the model of noise. We have used exact likelihood provided by CosmoMC for this analysis [63]. The parameter forecasts for $SA + \alpha + \beta$ model for both fiducial cosmologies are given in the corner plot 6. We have included the constraints obtained from $TTTEE + \text{lowl} + \text{lowE}$ for comparison. An enlarged view of joint confidence contours of α and β parameter is also given. We find that confidence contours of cosmological parameters are smaller for ECHO mission which illustrates its ability to arrive at tighter constraints. We find that, for FC-2 fiducial cosmology, forecasted values of α and β are $\alpha = 1.381 \times 10^{-2} \pm 3.286 \times 10^{-3}$ and $\beta = 2.651 \times 10^{-2} \pm 6.378 \times 10^{-3}$. Such a measurement can rule out null values for α and β by more than $4 - \sigma$. Further, it is evident from figure 6 that, when working with FC-1 the values of α and β are centred around zero. This establishes ability of future CMB missions such as ECHO to

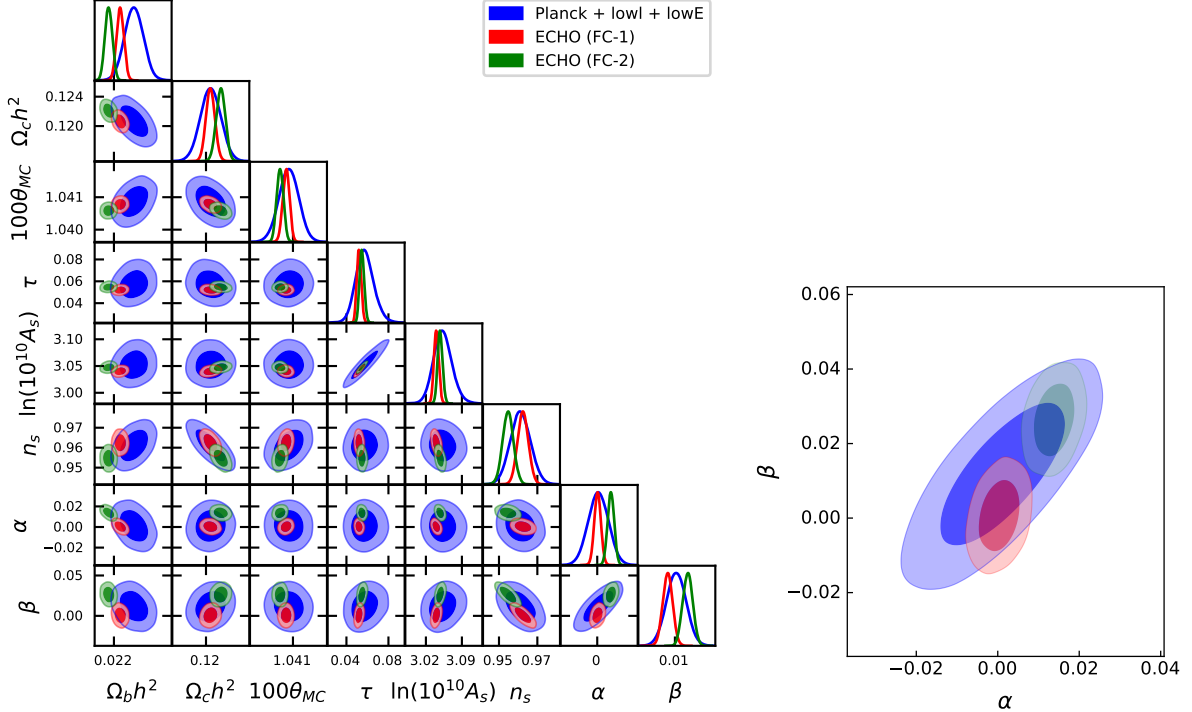


FIG. 6: Forecast for model parameters of $SA + \alpha + \beta$ model that can be obtained with ECHO mission is shown in the left. We have considered two fiducial cosmologies without (FC-1) and with (FC-2) power suppression at low multipoles. Forecast of joint posterior distribution of α and β has been magnified and plotted on the right. From right panel it is very much clear that the presence of power suppression can be estimated much more decisively from near-ultimate CMB missions such as ECHO.

make stronger conclusions about the presence of power suppression using simple phenomenological models that describe spectra at low multipoles. This is the final result of this paper.

VIII. SUMMARY AND DISCUSSION

A lack of power at low multipoles has been observed ever since the first measurement of temperature power spectrum by COBE [64]. Since then it has been confirmed by WMAP [65] and Planck missions. WMAP and Planck collaborations had also observed an inconsistency in the value of lensing parameter. Both these features depart from the predictions of standard model at the level of about $2 - 3\sigma$ only. Nevertheless, combined existence of these as well as other anomalies is intriguing. There have been several efforts to study models which could lead to suppression of power at low multipoles. Recently, it has also been pointed out that some models which lead to a suppression of power at low multipoles can also reduce the lensing tension. In this work, we investigated the connection between power suppression and lensing anomaly using simple extensions to standard scale invariant power spectrum (SA).

We considered three models namely (i) nearly scale invariant spectrum with a running of spectral index ($SA + \alpha$) (ii) nearly scale invariant spectrum with a running of running of spectral index ($SA + \beta$) and (iii) nearly scale invariant spectrum with both running and running of running of spectral index ($SA + \alpha + \beta$). These models are agnostic about power suppression. The priors we have considered in table I can equally generate a power spectrum with enhancement as well as suppression of power at low multipoles. It is true that, for these models, power suppression at low

multipoles implies an enhancement in power at higher multipoles. However, when limited to low multipoles, say $\ell \lesssim 2500$, the extended models mainly differ with SA in their behaviour at low multipoles. In this work, we are only interested in the behaviour of these models in this range of multipoles.

We performed four different analyses. First, we performed a Bayesian parameter estimation of these models with CMB temperature, polarisation, BAO and DES data sets. This analysis, described in section IV showed that, for extensions to SA , data selects model parameters which leads to a suppression of power at low multipoles. This is evident from our computations of $S_{1/2}$ given in table VI. Of the three models, $SA + \alpha + \beta$ leads to largest suppression followed by $SA + \beta$. We also see that, for these two models, addition of polarisation or BAO and DES data sets lead to parameters which lead to higher values of $S_{1/2}$ or lesser suppression of power. Secondly, we verified whether extensions to SA also lead to alleviation of lensing anomaly. We did this following two methods. In Method I, we did a Bayesian parameter estimation of extensions to SA after including A_L as a free parameter. In Method II, we fixed the parameters α and β to their marginalised mean value, obtained upon comparison with TT + lowl + lowE data, given in table II. We have chosen this data because it is the one with least error. In both methods, we find that lensing tension is reduced in $SA + \alpha + \beta$ and $SA + \beta$ models in the sense that compared to SA the value of $A_L = 1$ become more probable. When Method I is used, we find that though the mean value of A_L does not change much, its standard deviation increases and hence makes the value of $A_L = 1$ more likely. On the other hand, when Method II is used we find that mean value of A_L decreases, thus alleviating the lensing anomaly. From table VII, we see that, when working with TT + lowl + lowE, while the value of $A_L = 1$ is more than $2 - \sigma$ away for SA , it is within $2 - \sigma$ error bars in the case of $SA + \alpha + \beta$. For $SA + \beta$ model, which leads to a higher $S_{1/2}$ compared to $SA + \alpha + \beta$ model, the alleviation of lensing anomaly is not as high. Table VIII illustrates the effect of considering additional data. We conclude from the table that alleviation of lensing anomaly is less whenever the power suppression is lower.

Thirdly we approached the problem from the perspective of information criteria. We find that Akaike information criteria weakly prefers SA over $SA + \beta$ and $SA + \alpha + \beta$ models, see table IX. The preference slightly increases for SA against $SA + \alpha + \beta$ when polarisation data is used. Addition of BAO or DES do not affect the analysis. Bayesian information criteria penalises addition of extra parameters. This results in SA being strongly preferred against both $SA + \beta$ and even more so against $SA + \alpha + \beta$ models. However, if we limit the analysis of BIC to lowl data, the preference for SA against $SA + \beta$ becomes weak and that against $SA + \alpha + \beta$ becomes moderate, see table X. We believe that it is important to limit data to relevant multipoles when investigating relevance of a local feature such as power suppression.

From table VI we see that polarisation prefers parameters with lesser amount of power suppression. However, it should be underlined that measurement of polarisation by Planck is noisy, see figure 5. Hence, in the fourth analysis, we predict the constraints on model parameters that can be obtained by near-ultimate future CMB space mission such as ECHO. Since the noise in measuring polarisation by ECHO is much smaller than the signal, it can constrain parameters to a greater extent than Planck. Figure 6 provides our prediction of the posterior probability distribution of model parameters that can be obtained by ECHO. We considered two fiducial cosmologies, namely one without (FC-1) and another with power suppression (FC-2). We assumed a uniform white noise for our analysis. We find that if we assume a fiducial cosmology with power suppression, it is able to constrain α and β with null values excluded at more than $4 - \sigma$. This illustrates the ability of future CMB missions to ascertain the presence or absence of a power suppression at low multipoles with a simple $SA + \alpha + \beta$ model.

Thus, in this paper we have investigated the relation between primordial power suppression at long wavelengths, power suppression in CMB at low multipoles and lensing anomaly using simple

extensions to standard model. We show that data favours values of $SA + \alpha + \beta$ model that lead to power suppression at low multipoles which in turn alleviates lensing anomaly. We have used information criteria to present the limitations of the current data in ascertaining the presence of power suppression. Though we have used $SA + \alpha + \beta$ for this study, we do not advocate that this is the underlying model of early universe but have only used this as a convenient template. Finally and more importantly, this study establishes the need for advanced CMB missions such as ECHO and the ability of $SA + \alpha + \beta$ model to ascertain the presence of power suppression with such missions.

Acknowledgement

We acknowledge support from Anusandhan National Research Foundation (ANRF) for their support through Start-up Research Grant SRG/2021/001769. We acknowledge the use of PU HPC facility of the National Supercomputing Mission and thank Centre for Cyber Physical Systems, National Institute of Technology Karnataka, Surathkal for the financial support for the same.

-
- [1] Y. Akrami et al. Planck 2018 results. X. Constraints on inflation. *Astron. Astrophys.*, 641:A10, 2020.
 - [2] Jérôme Martin, Christophe Ringeval, Roberto Trotta, and Vincent Vennin. The Best Inflationary Models After Planck. *JCAP*, 03:039, 2014.
 - [3] Jerome Martin, Christophe Ringeval, and Vincent Vennin. Encyclopædia Inflationaris: Opiparous Edition. *Phys. Dark Univ.*, 5-6:75–235, 2014.
 - [4] A. Ijjas, P. J. Steinhardt, and A. Loeb. Cosmic inflation theory faces challenges. *Scientific American*, 316(2), 2017.
 - [5] A. Guth et al. A cosmic controversy. *Scientific American*, 316(5), 2017.
 - [6] Arno A. Penzias and Robert Woodrow Wilson. A Measurement of excess antenna temperature at 4080-Mc/s. *Astrophys. J.*, 142:419–421, 1965.
 - [7] C. L. Bennett, A. Banday, K. M. Gorski, G. Hinshaw, P. Jackson, P. Keegstra, A. Kogut, George F. Smoot, D. T. Wilkinson, and E. L. Wright. Four year COBE DMR cosmic microwave background observations: Maps and basic results. *Astrophys. J. Lett.*, 464:L1–L4, 1996.
 - [8] P. James E. Peebles, Lyman A. Page, and R. Bruce Partridge. *Finding the big bang*. 2009.
 - [9] N. Aghanim et al. Planck 2018 results. I. Overview and the cosmological legacy of Planck. *Astron. Astrophys.*, 641:A1, 2020.
 - [10] N. Aghanim et al. Planck 2018 results. VI. Cosmological parameters. *Astron. Astrophys.*, 641:A6, 2020. [Erratum: *Astron. Astrophys.* 652, C4 (2021)].
 - [11] Dominik J. Schwarz, Craig J. Copi, Dragan Huterer, and Glenn D. Starkman. CMB Anomalies after Planck. *Class. Quant. Grav.*, 33(18):184001, 2016.
 - [12] Y. Akrami et al. Planck 2018 results. VII. Isotropy and Statistics of the CMB. *Astron. Astrophys.*, 641:A7, 2020.
 - [13] Alexander Vilenkin and L. H. Ford. Gravitational Effects upon Cosmological Phase Transitions. *Phys. Rev. D*, 26:1231, 1982.
 - [14] Carlo R. Contaldi, Marco Peloso, Lev Kofman, and Andrei D. Linde. Suppressing the lower multipoles in the CMB anisotropies. *JCAP*, 07:002, 2003.
 - [15] Alexei A. Starobinsky. Spectrum of adiabatic perturbations in the universe when there are singularities in the inflation potential. *JETP Lett.*, 55:489–494, 1992.
 - [16] Rajeev Kumar Jain, Pravabati Chingangbam, Jinn-Ouk Gong, L. Sriramkumar, and Tarun Souradeep. Punctuated inflation and the low CMB multipoles. *JCAP*, 01:009, 2009.
 - [17] H. V. Ragavendra, Debika Chowdhury, and L. Sriramkumar. Suppression of scalar power on large scales and associated bispectra. *Phys. Rev. D*, 106(4):043535, 2022.
 - [18] Dhiraj Kumar Hazra, L. Sriramkumar, and Jerome Martin. BINGO: A code for the efficient computation of the scalar bi-spectrum. *JCAP*, 05:026, 2013.

- [19] V. Sreenath, Rakesh Tibrewala, and L. Sriramkumar. Numerical evaluation of the three-point scalar-tensor cross-correlations and the tensor bi-spectrum. *JCAP*, 12:037, 2013.
- [20] V. Sreenath, Dhiraj Kumar Hazra, and L. Sriramkumar. On the scalar consistency relation away from slow roll. *JCAP*, 02:029, 2015.
- [21] V. Sreenath and L. Sriramkumar. Examining the consistency relations describing the three-point functions involving tensors. *JCAP*, 10:021, 2014.
- [22] Simon Prunet, Jean-Philippe Uzan, Francis Bernardeau, and Tristan Brunier. Constraints on mode couplings and modulation of the CMB with WMAP data. *Phys. Rev. D*, 71:083508, 2005.
- [23] Christopher Gordon, Wayne Hu, Dragan Huterer, and Thomas M. Crawford. Spontaneous isotropy breaking: a mechanism for cmb multipole alignments. *Phys. Rev. D*, 72:103002, 2005.
- [24] Ivan Agullo, Javier Olmedo, and V. Sreenath. Observational consequences of Bianchi I spacetimes in loop quantum cosmology. *Phys. Rev. D*, 102(4):043523, 2020.
- [25] Ivan Agullo, Javier Olmedo, and V. Sreenath. Predictions for the Cosmic Microwave Background from an Anisotropic Quantum Bounce. *Phys. Rev. Lett.*, 124(25):251301, 2020.
- [26] Abhay Ashtekar, Brajesh Gupta, Donghui Jeong, and V. Sreenath. Alleviating the Tension in the Cosmic Microwave Background using Planck-Scale Physics. *Phys. Rev. Lett.*, 125(5):051302, 2020.
- [27] Abhay Ashtekar, Brajesh Gupta, and V. Sreenath. Cosmic Tango Between the Very Small and the Very Large: Addressing CMB Anomalies Through Loop Quantum Cosmology. *Front. Astron. Space Sci.*, 8:76, 2021.
- [28] Mercedes Martín-Benito, Rita B. Neves, and Javier Olmedo. Alleviation of anomalies from the nonoscillatory vacuum in loop quantum cosmology. *Phys. Rev. D*, 108(10):103508, 2023.
- [29] Ivan Agullo, Dimitrios Kranas, and V. Sreenath. Anomalies in the Cosmic Microwave Background and Their Non-Gaussian Origin in Loop Quantum Cosmology. *Front. Astron. Space Sci.*, 8:703845, 2021.
- [30] Ivan Agullo, Dimitrios Kranas, and V. Sreenath. Large scale anomalies in the CMB and non-Gaussianity in bouncing cosmologies. *Class. Quant. Grav.*, 38(6):065010, 2021.
- [31] Ivan Agullo, Dimitrios Kranas, and V. Sreenath. Anomalies in the CMB from a cosmic bounce. *Gen. Rel. Grav.*, 53(2):17, 2021.
- [32] Paola C. M. Delgado, Ruth Durrer, and Nelson Pinto-Neto. The CMB bispectrum from bouncing cosmologies. *JCAP*, 11:024, 2021.
- [33] Bartjan van Tent, Paola C. M. Delgado, and Ruth Durrer. Constraining the Bispectrum from Bouncing Cosmologies with Planck. *Phys. Rev. Lett.*, 130(19):191002, 2023.
- [34] Ivan Agullo, Boris Bolliet, and V. Sreenath. Non-Gaussianity in Loop Quantum Cosmology. *Phys. Rev. D*, 97(6):066021, 2018.
- [35] Vijayakumar Sreenath, Ivan Agullo, and Boris Bolliet. Computation of non-Gaussianity in loop quantum cosmology. In *15th Marcel Grossmann Meeting on Recent Developments in Theoretical and Experimental General Relativity, Astrophysics, and Relativistic Field Theories*, 4 2019.
- [36] Roshna K and V. Sreenath. Estimation of imprints of the bounce in loop quantum cosmology on the bispectra of cosmic microwave background. *JCAP*, 08:014, 2023.
- [37] Roshna K and V. Sreenath. Viability of loop quantum cosmology at the level of bispectrum. In *17th Marcel Grossmann Meeting: On Recent Developments in Theoretical and Experimental General Relativity, Gravitation, and Relativistic Field Theories*, 10 2024.
- [38] Erminia Calabrese, Anze Slosar, Alessandro Melchiorri, George F. Smoot, and Oliver Zahn. Cosmic Microwave Weak lensing data as a test for the dark universe. *Phys. Rev. D*, 77:123531, 2008.
- [39] Y. Akrami et al. Planck 2018 results. IX. Constraints on primordial non-Gaussianity. *Astron. Astrophys.*, 641:A9, 2020.
- [40] D. Sivia and J. Skilling. *Data Analysis: A Bayesian Tutorial*. Oxford University Press, Oxford, 2006.
- [41] Antony Lewis and Sarah Bridle. Cosmological parameters from CMB and other data: A Monte Carlo approach. *Phys. Rev. D*, 66:103511, 2002.
- [42] Antony Lewis, Anthony Challinor, and Anthony Lasenby. Efficient computation of CMB anisotropies in closed FRW models. *Astrophys. J.*, 538:473–476, 2000.
- [43] N. Aghanim et al. Planck 2018 results. V. CMB power spectra and likelihoods. *Astron. Astrophys.*, 641:A5, 2020.
- [44] D. N. Spergel et al. First year Wilkinson Microwave Anisotropy Probe (WMAP) observations: Determination of cosmological parameters. *Astrophys. J. Suppl.*, 148:175–194, 2003.
- [45] Florian Beutler, Chris Blake, Matthew Colless, D. Heath Jones, Lister Staveley-Smith, Lachlan Camp-

- bell, Quentin Parker, Will Saunders, and Fred Watson. The 6dF Galaxy Survey: Baryon Acoustic Oscillations and the Local Hubble Constant. *Mon. Not. Roy. Astron. Soc.*, 416:3017–3032, 2011.
- [46] Ashley J. Ross, Lado Samushia, Cullan Howlett, Will J. Percival, Angela Burden, and Marc Manera. The clustering of the SDSS DR7 main Galaxy sample – I. A 4 per cent distance measure at $z = 0.15$. *Mon. Not. Roy. Astron. Soc.*, 449(1):835–847, 2015.
 - [47] Donald G. York et al. The Sloan Digital Sky Survey: Technical Summary. *Astron. J.*, 120:1579–1587, 2000.
 - [48] T. M. C. Abbott et al. The Dark Energy Survey Data Release 1. *Astrophys. J. Suppl.*, 239(2):18, 2018.
 - [49] E. Morganson et al. The Dark Energy Survey Image Processing Pipeline. *Publ. Astron. Soc. Pac.*, 130(989):074501, 2018.
 - [50] B. Flaugher et al. The Dark Energy Camera. *Astron. J.*, 150:150, 2015.
 - [51] H. Akaike. A new look at the statistical model identification. *IEEE Trans. Automatic Control*, 19(6):716–723, 1974.
 - [52] Gideon Schwarz. Estimating the Dimension of a Model. *Annals Statist.*, 6:461–464, 1978.
 - [53] S. Capozziello, R. D’Agostino, and O. Luongo. High-redshift cosmography: auxiliary variables versus Padé polynomials. *Mon. Not. Roy. Astron. Soc.*, 494(2):2576–2590, 2020.
 - [54] J. P. Hu and F. Y. Wang. High-redshift cosmography: Application and comparison with different methods. *Astron. Astrophys.*, 661:A71, 2022.
 - [55] J. Delabrouille et al. Exploring cosmic origins with CORE: Survey requirements and mission design. *JCAP*, 04:014, 2018.
 - [56] Philippe André et al. PRISM (Polarized Radiation Imaging and Spectroscopy Mission): An Extended White Paper. *JCAP*, 02:006, 2014.
 - [57] Shaul Hanany et al. PICO: Probe of Inflation and Cosmic Origins. 3 2019.
 - [58] LLOYD Knox. Determination of inflationary observables by cosmic microwave background anisotropy experiments. *Phys. Rev. D*, 52:4307–4318, 1995.
 - [59] Max Tegmark. CMB mapping experiments: A Designer’s guide. *Phys. Rev. D*, 56:4514–4529, 1997.
 - [60] Jussi Valiviita. Power Spectra Based Planck Constraints on Compensated Isocurvature, and Forecasts for LiteBIRD and CORE Space Missions. *JCAP*, 04:014, 2017.
 - [61] Debabrata Adak, Aparajita Sen, Soumen Basak, Jacques Delabrouille, Tuhin Ghosh, Aditya Rotti, Ginés Martínez-Solaesche, and Tarun Souradeep. B-mode forecast of CMB-Bhārat. *Mon. Not. Roy. Astron. Soc.*, 514(2):3002–3016, 2022.
 - [62] J. Tauber et al. The Scientific programme of Planck. 4 2006.
 - [63] Samira Hamimeche and Antony Lewis. Likelihood Analysis of CMB Temperature and Polarization Power Spectra. *Phys. Rev. D*, 77:103013, 2008.
 - [64] G. Hinshaw, A. J. Banday, C. L. Bennett, K. M. Gorski, Alan Kogut, C. H. Lineweaver, George F. Smoot, and E. L. Wright. 2-point correlations in the COBE DMR 4-year anisotropy maps. *Astrophys. J. Lett.*, 464:L25–L28, 1996.
 - [65] C. L. Bennett et al. First year Wilkinson Microwave Anisotropy Probe (WMAP) observations: Preliminary maps and basic results. *Astrophys. J. Suppl.*, 148:1–27, 2003.